



Aerodynamic analysis of basic and extended lead-trail formation using numerical technique

M. Gunasekaran^{a,*}, Rinku Mukherjee^b

^a Department of Mechanical Engineering, SRM Institute of Science and Technology, Chennai, 603202, India

^b Department of Applied Mechanics, Indian Institute of Technology Madras, 600036, India

ARTICLE INFO

Article history:

Received 26 February 2019

Received in revised form 1 November 2019

Accepted 7 November 2019

Available online 13 November 2019

Keywords:

Formation

Lead-trail

Configuration

Post-stall

Fuel-savings

Decambering

ABSTRACT

This paper uses a numerical post-stall predictive tool based on ‘deambering’ approach to study the aerodynamic characteristics of a lead-trail formation in pre and post-stall flow conditions. A basic lead-trail formation consisting of 2 wings and an extended formation consisting of 5 wings are studied with a view to the possibility of fuel savings, increase in range of operation, delayed flow separation and efficient positioning of the wings with respect to each other. Whether increasing the number of wings in a configuration is more useful is also looked into. The optimum operational angles of attack for maximum advantage in terms of fuel efficiency of all wings is studied including post-stall angles of attack. Numerical results for C_L , C_{D_i} , section C_l distribution and their dependence on vertical offsets and angle of attack are reported.

© 2019 Elsevier Masson SAS. All rights reserved.

1. Introduction

Formation flight is one of the way of flying with more than single aircraft in a disciplined and controlled manner. In a tight formation such as is seen in an airshow, the aircraft may fly together with few meters apart and must have the excellent coordination between the leader and following aircraft. The main aim of flying in a group is the energy savings which comes from the utilization of wing tip vortices. The example of such formation observed in birds and aircraft are shown in Fig. 1. While birds fly in formation to conserve energy, aircraft save a considerable amount of energy in the form of fuel when they are flying in formation.

Lead-trail formation as the name implies, the leading flight is followed directly behind by trailing aircraft which maintains some specific distance, typically 1 nm. There are two types of configuration, basic and extended lead-trail, in which extended lead-trail formations may be used when greater maneuverability is desired.

The lead-trail formation may be observed in fixed wing aircraft when it is used for air-to-air refueling. The illustrative example of such configuration shown in Fig. 1(b) is to do air-to-air refueling from Boeing 707 of the Imperial Iranian air force to an IIAF Boeing 747.

Modern scientists have been attracted by formation flying as the aircraft flying formation has certain aerodynamic advantages.

An upwash field is created by the leading aircraft, which helps to save considerable amount of fuel when trailing aircraft flying in the upwash. This advantage is both for leading and trailing aircrafts since bound and trailing vortex system of trailing aircraft affects the leading aircraft in formation.

Formation flying attracting the attention of scientists for some time now as an aircraft flying in formation has certain aerodynamic advantages. A significant saving in the fuel can be obtained by flying in the upwash field created by the leading aircraft. This advantage is not just limited to the trailing aircraft but also to the leading aircraft, which is also affected by the bound and trailing vortex system of the trailing aircraft.

Many projects in the science and observation domains involve the use of formation flying to ensure the mission performance. Also, simple designs consisting of two satellites in a lead-trail formation seems to be sufficient for a broad range of applications like interferometry, geodesy, etc. Martinot and Rozanes [1] worked on the station keeping the phase of lead-trail formations in Low-Earth orbits. The station keeping criterion mainly evolves under the differential effect of the atmospheric drag between the trailing and leading satellites.

Buzogany [2] stated that the trail formation(lead-trail) is important since a minimum amount of land mass is overflown by the formation aircraft, translating to a reduced probability of detection by ground forces. He further investigated various manoeuvres performed during the formation by change in the velocity, heading, altitude, or a combination of the three. It is also included that for reducing the amount of fuel consumption, pilot's may change altitude in addition to the heading change.

* Corresponding author.

E-mail address: aerogunasekar@gmail.com (M. Gunasekaran).

Nomenclature

$C_{lsec}, C_{msec}, C_{d_{i_{sec}}}$	2D section coefficients of lift, pitching moment and induced drag
$C_{L_{max}}$	Maximum Lift coefficient
$C_{d_{i_{min}}}$	Minimum Induced Drag coefficient
C_L, C_M, C_{D_i}	3D wing coefficient of lift, pitching moment and induced drag
$(L/D)_{max}$	Maximum lift-to-drag ratio
c	Airfoil/wing chord length
α	Angle of Attack
$\alpha_{C_L=0}$	Zero-lift angle of attack
$\Delta C_L, \Delta C_M$	Difference between viscous and potential coefficients of lift and pitching moment
δ_1, δ_2	Decambering functions
x_1, x_2	Cartesian locations of δ_1 and δ_2
θ_1, θ_2	Spherical locations of δ_1 and δ_2
dz	Spherical offset between wings in configuration

Subscript

lw, tw	Leading wing, trailing wing
lw-twi	Vertical offset between leading wing and trailing wing 'i', $i = 1:4$

Birds fly organized in groups do so in one of two fashions as shown by Bajec and Heppner [3], namely, Line formations and Cluster formations. The line formations are typically demonstrated by large birds like waterfowl, where birds fly arranged in single lines, often joined. Cluster formations are usually made up of large numbers of smaller birds like pigeons or blackbirds flying in more irregular arrangements that have a strong three-dimensional character.

Cutts and Speakman [4] predicted on communication hypothesis that wing tip spacing and depth should be positively related to providing information on the position. Response times for shifts between flapping and gliding were negatively related to flock size, and were shorter in V and J formations than in column and echelon formations.

New methodologies have been developed for determining the aerodynamic characteristics generated in formation. King and Gopalathnam [5] developed a method for determining the optimum downwash when two aircraft flying in formation.

They calculated the theoretical induced drag benefits for ideally loaded wings flying in formation and ground effect, and it is been shown that the elliptically loaded wing structures have nearly the same drag as optimally loaded wing configurations. From this study, they revealed that the optimum lateral separation is 10% of wingspan between the wing tips. In this position, a formation of 25 elliptically loaded wings flying out of ground effect experiences 81% drag reduction compared to 25 wings flying in isolation.

Many geometric parameters of wing may influence the performances of the flight. These performances may not be limited to single wing aircraft and it may be extended to the formation flight as well. Thien and Moelyadi [6] used domain discretization and flow field properties evaluation to explain the effect of incidence angle, dihedral angle, aspect ratio and taper ratio in V-formation flight. They found that aspect ratio has a significant effect on increasing the rear wing lift and pitching moment, but seems to have no effect on the drag reduction.

Many species of large birds have been investigated when they are flying in formation. This is because of flight power demands and energy expenditure could be reduced if they fly at optimal spacing. Weimerskirch et al. [7] measured the heart beat of birds when flying and gliding, and proved that they save a considerable amount of energy while flying in V formation.

These benefits may be gained in formation flight by changing the offsets between two aircraft and by altering the lift distribution along the wing span in leading aircraft which influences trailing wing(tw) aerodynamic characteristics.

The present authors have also worked on other configurations like Chevron and Echelon and shown that each configuration has its advantages. In this particular work the authors are engaged in studying the maximum benefit of the 'lead-trail' configuration.

Now, in the context of operating at high and post-stall angles of attack, the present 'lead-trail' configuration is tested to achieve the maximum C_L for all wings in the configuration. For this, a basic 'lead-trail' configuration consisting of two wings, where each wing has a section NACA2412 with $\alpha_{stall} \approx 15^\circ$ and $C_{L_{max}} \approx 1.5$ is tested in such a way so as to maximize the C_L to be achieved for both wings. It is understood that higher the C_L achieved for the configuration will result in better fuel savings.

The leading wing is at $\alpha_{lw} = 8^\circ$ and the trailing wing is operated at pre to post-stall angles of attack, $8^\circ < \alpha \leq 24^\circ$. The distribution of the effective angle of attack, α_{eff} and C_L for this configuration is shown in Fig. 2a. It is found that the trailing wing stalls at $\alpha = 24^\circ$ and hence, the configuration cannot be operated at ($\alpha_{lw} = 8^\circ, \alpha_{tw} = 24^\circ$).

However, if the leading wing angle of attack is increased further to near-stall, $\alpha_{lw} = 15^\circ$, the trailing wing at $\alpha_{tw} = 24^\circ$



(a) Formation in birds



(b) Formation in aircrafts

Fig. 1. Examples of formation flying.

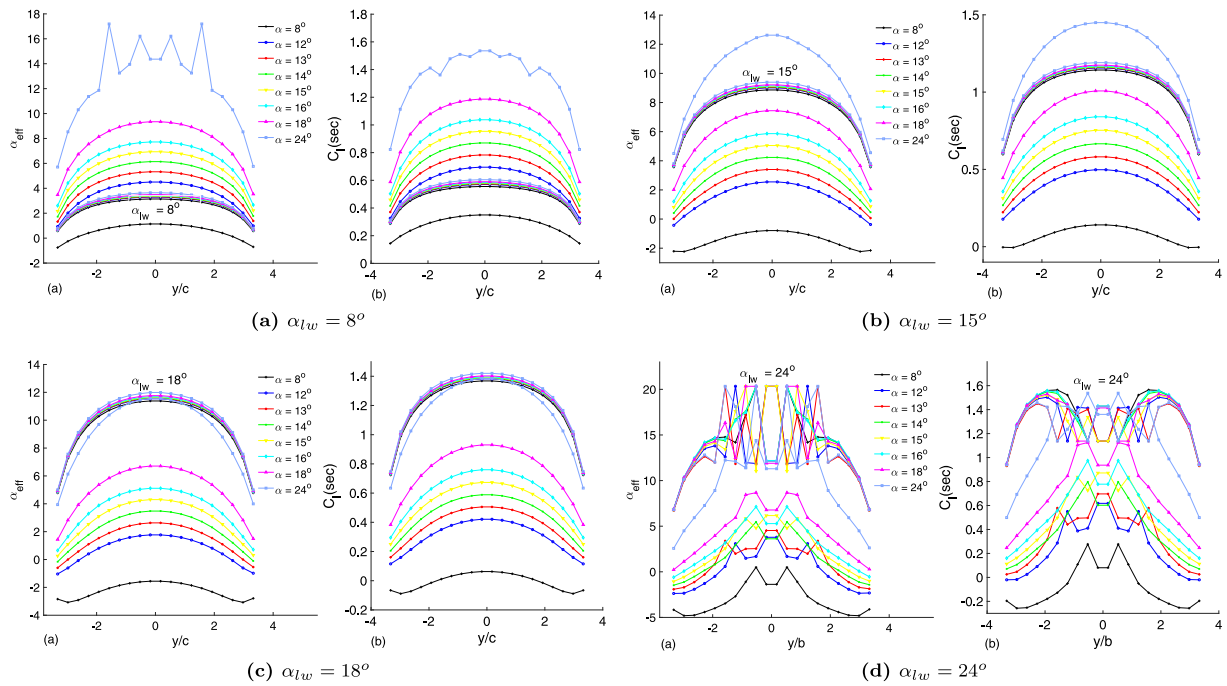


Fig. 2. 2-wing configuration: $\alpha_{eff} - y/b$ and $C_l - y/b$.

does not stall anymore as shown in Fig. 2b and the $C_{l_{max}}$ penalty of the trailing wing is not significant as $C_{l_{max}} \approx 1.45$. In addition, the leading wing is also operating at a much higher $C_{l_{max}} \approx 1.2$ as shown in Fig. 2b compared to $C_{l_{max}} \approx 0.56$ for $\alpha_{lw} = 8^\circ$ as shown in Fig. 2a. With further increase in the angle of attack of the leading wing to $\alpha_{lw} = 18^\circ$, its $C_{l_{max}} \approx 1.42$ and the trailing wing is still operating at $\alpha_{tw} = 24^\circ$ with $C_{l_{max}} \approx 1.38$ as shown in Fig. 2c. At $\alpha_{lw} = 24^\circ$, both the wings stall as shown in Fig. 2d and this configuration cannot be used for operation.

Clearly, it is advantageous to operate at high and post-stall angles of attack with increased C_l but this is possible only when the wings operate in a configuration, which in this case is ‘lead-trail’. The same wings when operating individually will stall at such high angles of attack.

Therefore, the motivation for this work stems from the fact that operating at high and post-stall angles of attack in a ‘lead-trail’ configuration has the possibility of increased fuel savings as they operate at high C_l s without flow separation.

2. Numerical procedure

A vortex-lattice method algorithm based on the decambering approach of Mukherjee and Gopalarathnam [8] is used for predicting formation flight aerodynamics of wings using known section data. Although the numerical code, VLM3D based on this approach was originally developed with a view to predict post-stall aerodynamics of single wings or their configurations, it has been found to be robust and powerful in the analysis of formation flight as well with some modifications.

The ability to change spatial offsets (chord-wise, span-wise and vertical), the ability to change the angle of attack of the trailing aircraft for a particular angle of attack of the leading aircraft and vice versa are incorporated into VLM3D to study formation flight aerodynamics. The unique feature of formation flight is the interaction between the vortices and aircraft (both leading and trailing), which is captured well by the modified VLM3D developed by Gunasekaran and Mukherjee [9]. Post-stall results provide an enhanced understanding of formation flight aerodynamics.

The code VLM3D based on the decambering approach was developed wherein the chordwise camber distribution at each section of the wing was reduced to account for the viscous effects at high angles of attack. The approach uses either or both C_l and C_m section data and uses a two-variable function for the decambering.

In addition, unlike all earlier methods, the approach uses a multi-dimensional Newton iteration that accounts for the cross-coupling effects between the sections in predicting the decambering for each step in the iteration. The subsequent discussion illustrates briefly the decambering approach by describing its application to model a two-dimensional flow past an example airfoil. The iterative approach for three-dimensional geometries is discussed next.

The primary methodology of ‘decambering’ used here has been developed by Mukherjee and Gopalarathnam [8]. However, while the focus of this work was to use the ‘decambering’ concept to model separated flow at high angles of attack, the objective of the present work is to study the interference effect of more than one wing operating together at a range of low to post-stall angles of attack. In the present work, therefore, when operating at post-stall angles of attack, the separated flow effects are modeled using the ‘decambering’ concept.

In the present work, the in-house code based on the ‘decambering’ methodology is modified where each of the multiple lifting surfaces operate as individual entities and affect each other. Using multiple wings increases the computational cost as well. Using multiple wings also means that at a single instance of time only one or some wings may stall and others may not. Hence, the ‘decambering’ approach needs to be selectively implemented.

Gunasekaran and Mukherjee [10] studied the effect of geometric and aerodynamic twist on an echelon configuration flight. Essentially, the twist changes the distribution of the effective angle of attack over the wing span and this affects wing performance including stall behavior.

This present paper studies a lead-trail configuration, the primary difference with the echelon configuration being that a wing in the lead-trail configuration will never experience asymmetric load distribution along wing span unlike in an echelon formation.

And the wing twist in the echelon formation is able to erase such asymmetric load distributions and prevents rolling moments. The lead-trail configuration, on the other hand is able to achieve higher C_L for each wing since stall is delayed, therefore suggesting decrease of fuel usage.

2.1. Application to 2D flow

The overall objective was to arrive at a scheme for incorporating the nonlinear section lift curves in wing analysis methods such as lifting line theory, discrete-vortex Weissinger's method and vortex lattice methods. For this purpose, it was assumed that the two-dimensional data $C_l - \alpha$ and $C_m - \alpha$ for the sections forming the wing were available from either experimental or computational results. The objective was that for the final solution of the 3D flow, the Γ distribution across the span would be consistent with the distribution of the effective α for each section and the C_l and C_m for each section would be consistent with the effective α for that section and the section $C_l - \alpha$ and $C_m - \alpha$ data.

This overall objective was achieved by finding the effective reduction in the camber distribution for each section along the span illustrated in Fig. 3. The typical flow past an airfoil at small angles of attack consists of a thin boundary layer that remains attached to the surfaces of the airfoil. For these conditions, the C_l and C_m predicted using potential flow analysis of the airfoil camberline agrees closely with the computational and experimental results that account for viscosity.

With increasing angles of attack, the boundary layer thickens on the upper surface and finally separates. It is this flow separation that causes the viscous results for C_l and C_m to deviate from the predictions using potential flow theory. The reason for the deviation can be related to the effective change in the airfoil camber distribution due to the boundary-layer separation. If the decambering could be accounted for, then a potential-flow prediction for the decambered airfoil would closely match the viscous C_l and C_m for the high- α flow past the original airfoil shape. This decambering idea served as the basis for the formulation of the current approach for the three-dimensional flow problem.

While the camber reduction due to the flow separation can be determined from computational flows, no such detailed information is available from wind tunnel results that typically provide only the $C_l - \alpha$ and $C_m - \alpha$ curves.

In the current method, the effective decambering for an airfoil was approximated using a function of two variables δ_1 and δ_2 . The two linear functions were superposed to obtain the final decambering function. Two variables were used because the decambering was being backed out from two pieces of information: the C_l and C_m from the airfoil data for the α under consideration. This approximation will, of course, not match the actual viscous decambering, but the objective was to find an equivalent camber reduction to match the viscous C_l and C_m for the α under consideration.

The effects of δ_1 and δ_2 on the change in C_l and C_m for a given α can be computed reasonably well using thin airfoil theory and a three-term Fourier series approximation for a flat plate with a flap deflection [12] as shown in Fig. 3. In the current work, x_2 was arbitrarily assumed to be 0.8, although any value from 0.5 to 0.9 seemed to work well.

To verify the effectiveness of the decambering approach, the values of δ_1 and δ_2 were calculated for the viscous $C_l - \alpha$ and $C_m - \alpha$ data and were then applied as a correction to the flat-plate camberline for potential flow analysis of the NACA-0012 airfoil using a lumped vortex method [8]. Fig. 4 shows the comparison of the predicted potential flow $C_l - \alpha$ for the decambered airfoil with the viscous result from XFOIL analysis. The agreement is seen to be very good, which verified that the two-variable decambering function can be used to model nonlinear lift as well as pitching moment curves for high angles of attack.

2.2. Application to a finite 3D wing

The objective here is to incorporate the two-variable decambering function into a three-dimensional analysis method such as a vortex lattice method (VLM) in an iterative fashion. And the advantage of using a method like VLM is that one can use more than one lifting surface, which in this particular case is two Cessna 172 wings in a Lead-trail and extended Lead-trail formations. The original algorithm of the VLM3D has therefore been modified for the current purpose, which is described in the following sections.

As in a typical VLM, each wing is divided into several spanwise, and chordwise panels and each panel correspond to a horseshoe vortex. In the current approach, the geometry of each spanwise section j of each wing is modified using local decambering variables, δ_{1j} and δ_{2j} . In both the cases of two-dimensional and three-dimensional, δ_1 and δ_2 were selected to match the difference between the potential-flow and the viscous-flow results. And in particular in the three-dimensional case, changing a δ on one section only say, the leading wing(lw) **A** will also affect the neighboring sections of wing **A** itself as well as all the sections on the downstream wing **B** and vice versa.

To account for these effects, a 2N-dimensional Newton iteration is used to predict the δ_1 and δ_2 at each of the N sections accounting for both wings so that the ΔC_l and ΔC_m at these sections approach zero with an increasing number of iterations. It is to be noted here that N accounts for a total number of sections on both wings, i.e. $\mathbf{N} = \mathbf{N}_A + \mathbf{N}_B$, where **A** and **B** denote the two wings. A 2NX2N matrix equation has to be solved for each step of the Newton iteration explained by Press et al. [13]), as shown in Eq. (1).

$$J \cdot \delta x = -F \tag{1}$$

$$J = \begin{pmatrix} J_{l1} & J_{l2} \\ J_{m1} & J_{m2} \end{pmatrix} = \begin{pmatrix} (J_{lA} + J_{lB})_1 & (J_{lA} + J_{lB})_2 \\ (J_{mA} + J_{mB})_1 & (J_{mA} + J_{mB})_2 \end{pmatrix} \tag{2}$$

$$(J_{l1})_{i,j} = \frac{\partial \Delta C_{li}}{\partial \delta_{1,j}} = (J_{lA} + J_{lB})_{i,j} = \frac{\partial (\Delta C_{lA} + \Delta C_{lB})}{\partial \delta_{1A}} + \frac{\partial (\Delta C_{lA} + \Delta C_{lB})}{\partial \delta_{1B}} \tag{3}$$

$$(J_{m1})_{i,j} = \frac{\partial \Delta C_{mi}}{\partial \delta_{1,j}} = (J_{lA} + J_{lB})_{i,j} = \frac{\partial (\Delta C_{mA} + \Delta C_{mB})}{\partial \delta_{1A}} + \frac{\partial (\Delta C_{mA} + \Delta C_{mB})}{\partial \delta_{1B}} \tag{4}$$

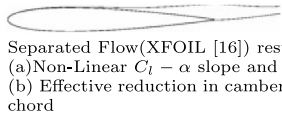
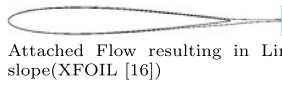
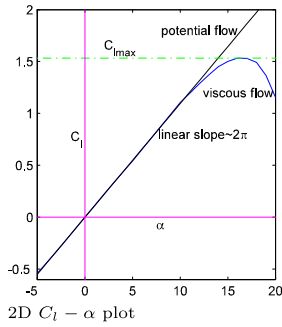
$$(J_{l2})_{i,j} = \frac{\partial \Delta C_{li}}{\partial \delta_{2,j}} = (J_{lA} + J_{lB})_{i,j} = \frac{\partial (\Delta C_{lA} + \Delta C_{lB})}{\partial \delta_{2A}} + \frac{\partial (\Delta C_{lA} + \Delta C_{lB})}{\partial \delta_{2B}} \tag{5}$$

$$(J_{l2})_{i,j} = \frac{\partial \Delta C_{li}}{\partial \delta_{2,j}} = (J_{lA} + J_{lB})_{i,j} = \frac{\partial (\Delta C_{lA} + \Delta C_{lB})}{\partial \delta_{2A}} + \frac{\partial (\Delta C_{lA} + \Delta C_{lB})}{\partial \delta_{2B}} \tag{6}$$

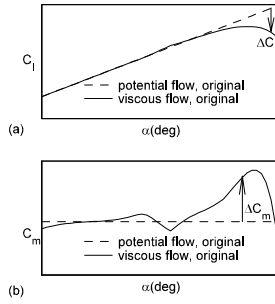
$$(J_{m2})_{i,j} = \frac{\partial \Delta C_{mi}}{\partial \delta_{2,j}} = (J_{mA} + J_{mB})_{i,j} = \frac{\partial (\Delta C_{mA} + \Delta C_{mB})}{\partial \delta_{2A}} + \frac{\partial (\Delta C_{mA} + \Delta C_{mB})}{\partial \delta_{2B}} \tag{7}$$

$$\alpha_{sec} = \frac{(C_l)_{sec}}{2\pi} - \delta_1 - \delta_2 \left[1 - \frac{\theta_2}{\pi} + \frac{\sin \theta_2}{\pi} \right] \tag{8}$$

where F is a 2N-dimensional vector containing the residuals of the functions f_i to be zeroed, i.e. ΔC_l and ΔC_m , δx is the 2N-dimensional vector containing the corrections required to the 2N variables x_i , i.e. δ_1 and δ_2 to bring the vector F closer to zero and



Viscous Flow Separation results in non-linear $C_l - \alpha$ curve



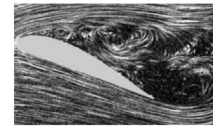
Schematic representation of residuals

$$\delta_2 = \frac{\Delta C_m}{\frac{1}{4} \sin 2\theta_2 - \frac{1}{2} \sin \theta_2}$$

$$\delta_1 = \frac{\Delta C_l - [2(\pi - \theta_2) + 2 \sin \theta_2] \delta_2}{2\delta_2}$$

$$\theta_2 = \cos^{-1}(1 - 2x_2); x_2 = 0.8$$

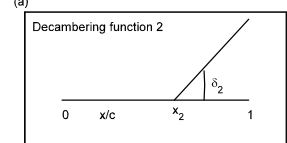
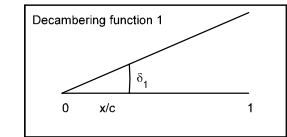
Thin Airfoil Theory: 3 term Fourier Series



(i) Experiment (https://commons.wikimedia.org/wiki/Category:Flow_separation#/media/File:Flow_separation.jpg)



(ii) Numerical Analysis using XFOIL [16]



(iii) Numerical Model Based on 'Decambering' Separated Flow Visualisation

Fig. 3. Overview of 2D decambering [11].

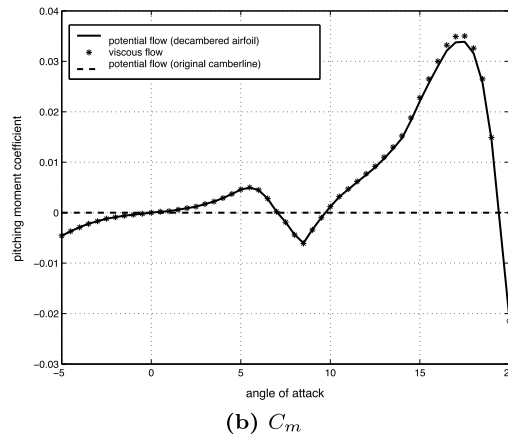
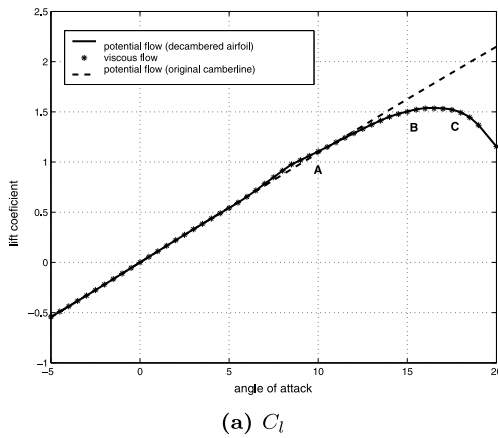


Fig. 4. Effectiveness of the decambering method.

J is the $2N \times 2N$ Jacobian of the system containing the gradient information.

For each step of the iteration, F and J are determined, and δx is computed using Eq. (1). The corrections are then applied to the variables to bring the residuals closer to zero. In the current scheme, the residual functions f_i were the values of the ΔC_l and ΔC_m for each of the wing sections, and the variables x_i were the values of δ_1 and δ_2 for each of the sections. The Jacobian can be partitioned into four submatrices as shown in Eq. (2). Eqs. (3)–(7) show the elements of the four sub matrices.

The iteration procedure can be summarized as follows:

1. Assume starting values of δ_1 and δ_2 for each section of the wing.
2. Compute the wing aerodynamic characteristics using the VLM code.
3. Compute the local section effective angles of attack (α_{sec}) using the local section $(C_l)_{sec}$ and Eq. (10). It is to be noted here that in Eq. (10), the variables δ_1 , δ_2 and θ_2 are defined for each section of the wing and are equivalent to those used earlier for the two-dimensional case in Eqs. (1)–(3).

4. Compute the residuals $\Delta C_l = (C_l)_{visc} - (C_l)_{sec}$ and $\Delta C_m = (C_m)_{visc} - (C_m)_{sec}$. The $(C_l)_{visc}$ and $(C_m)_{visc}$ are obtained from the known section data for the angle of attack corresponding to α_{sec} .
5. Calculate the Jacobian matrix for the Newton iteration.
6. Solve matrix Eq. (4) to obtain the perturbations to δ_1 and δ_2 at each section and update values of δ_1 and δ_2 .
7. Repeat steps 2–6 until ΔC_l and ΔC_m are close to zero within a specified tolerance.

It must be mentioned that for cases where the experimental/computational viscous data for the airfoil section does not have C_m or for cases where the decambering approach is applied to an analysis method that cannot compute the section pitching moments (e.g. LLT or a discrete-vortex Weissinger's method), the decambering is modeled as a function of a single variable δ_1 ; δ_2 is assumed to be set to zero. In this case, the viscous decambering function becomes similar to the α reduction approach used in Refs. 8 and 9. However, in the current approach, the cross coupling between the sections was still accounted for in predicting the δ_1 values for the next step. In the earlier approaches, the

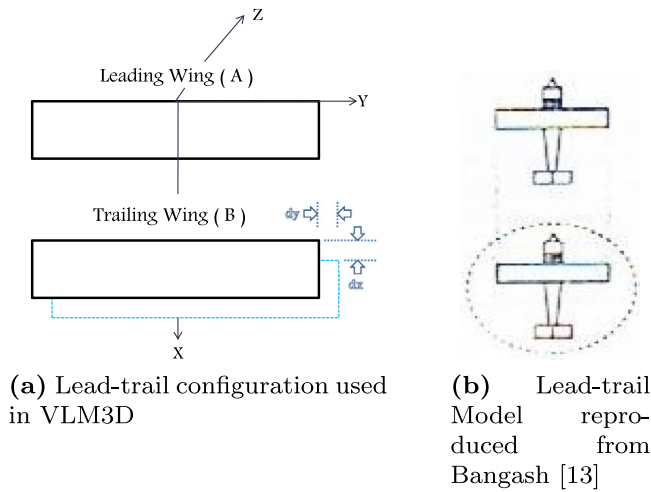


Fig. 5. Lead-trail configuration used in VLM3D & experiment.

sections are assumed to be decoupled, and the δ_1 values for each section are predicted using just the local values of the ΔC_l . For this reason, it is believed that the current method will be more effective in handling situations where the section flows are closely coupled.

3. Results & discussion

In lead-trail formation, the effect of wingtip vortices are slightly different from the other formations since the trailing wing in lead-trail formation is just behind the leading wing with some distances in the stream wise direction. Here, the whole trailing wing comes in the region of downwash instead of upwash since the tip vortices of leading wing are exactly in the same direction as that of trailing wing.

The results based on basic Lead-Trail and extended formations using current method are presented and compared with the experimental results of Bangash [14]. The rectangular wings are used in both leading and trailing wings of this formation. The dimensions of rectangular wing are, spanlength, $b = 7$ and with an aspect ratio, $(AR) = 7$. The trailing wing is placed at four chord length distances just behind the leading wing and the wingtip vortices of trailing wing are exactly in the same direction as that of leading wing. The configurations used both in experiment and current methods are shown in Fig. 5.

The in-house code used here, VLM3D requires the 2D $C_l - \alpha$ and/or $C_m - \alpha$ data as input to predict the aerodynamic characteristics of the 3D wing(s). Hence, the output is tested for different input data, namely numerical and experiments to test its feasibility and repeatability.

The 2D data from experiments of Bangash [14] is not available. Hence, the available 3D $C_l - \alpha$ is used as input and the wing is now set as an infinite wing, i.e. with infinite span in VLM3D. The resulting output is taken as the 2D data.

3.1. Analysis of the aerodynamic performance of the basic 2-wing lead-trail configuration

For understanding the aerodynamic performances of the wings in a lead-trail configuration, parameters like vertical offsets, which represent the location of the wings with respect to each other and their angles of attack are studied. Three different vertical offsets, i.e. $dz = -0.11, 0.33$ and 0.78 are used, while the other two offsets are fixed, i.e. $dx = 0$ and $dy = 0$. The trailing wing angle of attack undergoes a sequence, $\alpha_{tw} = -5^\circ$ to 30°

while the leading wing angle of attack, $\alpha_{lw} = 8^\circ$ is fixed. For each of the vertical offsets, four sets of input data were used, i.e. (i) NACA2412 data [15] (ii) VLM3D data without $C_m - \alpha$ (iii) VLM3D data with $C_m - \alpha$ (iv) 2D data generated from 3D experiments [14] and (v) 2D data of Selig [16].

The effect of using different input 2D data on the trailing wing at a given vertical offset is studied where the $C_l - \alpha$ is calculated for the trailing wing for input data (i), (ii) and (iii) shown in Fig. 6 for three different vertical offsets.

For a vertical offset, $dz = -0.11$ and $dz = 0.33$ shown in Fig. 6(a) and (b), the 3D $C_l - \alpha$ using input data both with and without $C_m - \alpha$ predicted by the current method show lower stall angles and not so distinct linear slope compared with experiment. However, for $dz = 0.33$, agreement of the current $C_l - \alpha$ with experiment at post-stall is quite encouraging. For the vertical offset, $dz = 0.78$ shown in Fig. 6(c), the results predicted by current method show some deviations with experiment in pre-stall and post-stall regions while there is no major disagreement with the prediction of α_{stall} . In all three cases, $C_l - \alpha$ predicted with $C_m - \alpha$ as input shows a lesser zero-lift angle of attack. Therefore, adding $C_m - \alpha$ along with $C_l - \alpha$ in the input becomes important to know the slope of the $C_l - \alpha$ curve and zero-lift angle of attack, α_{0L} .

The stall angle observed in experiment at $dz = -0.11$ is significantly higher than that predicted by the current method. With increase in the vertical offset, this difference becomes lesser and the α_{stall} predicted by the current method is almost same as in experiment at $dz = 0.78$. Also, at post stall, compared to experiment, the current method shows a smoother curve with several data points.

The section C_l distribution is calculated for the trailing wings for input data (ii), (iii) and (iv) shown in Fig. 7 for three different vertical offsets at four selected angles of attack of the trailing wing. For all the vertical offsets used here, both the leading wing and the trailing wing show different section C_l for different input data used except at the lower angles of attack, $\alpha_{tw} = -2^\circ$ and $\alpha_{tw} = 6^\circ$, when the section C_l predicted using input data (iii) and (iv) coincide. For all cases, only input data (iv) predicts stall at $\alpha_{tw} = 22^\circ$.

This is emphasized further by studying the effect of vertical offsets on section C_l distribution on the trailing wing for a given input data shown in Fig. 8. As observed even at $\alpha = 24^\circ$, a change in vertical offset does not predict stall when input data (iv) is used shown in Fig. 8(a). However, for all the three vertical offsets used here, both input data (i) and (v) predict stall at $\alpha = 24^\circ$, although their nature is different.

The effect of different input data, vertical offsets and angle of attack of the trailing wing on the maximum section C_l at root section is summarized in Fig. 9 and it is observed that a change in the vertical offsets affects only the input data (v) significantly. The most dominant factor is the angle of attack.

3.2. Analysis of the aerodynamic performance of an extended 5-wing lead-trail configuration

In this section, a lead-trail formation of 5 wings shown in Fig. 10 is analyzed. The aspect ratio of the wings are same as in the basic lead-trail formation of 2 wings. The airfoil data used here for all the wings is that of NACA2412 [15]. The effect of vertical offsets on trailing wings for a given angle of attack of the leading wing, α_{lw} is studied.

The $C_l - \alpha$ and $C_{D_i} - \alpha$ for a configuration, where all the trailing wings are below or above the leading wing, i.e. for negative and positive vertical offsets, the magnitude of the offsets being same is shown in Figs. 11a and 11b respectively. The vertical offsets are $dz_{lw-tw1} = \pm 0.11$, $dz_{lw-tw2} = \pm 0.22$, $dz_{lw-tw3} = \pm 0.33$

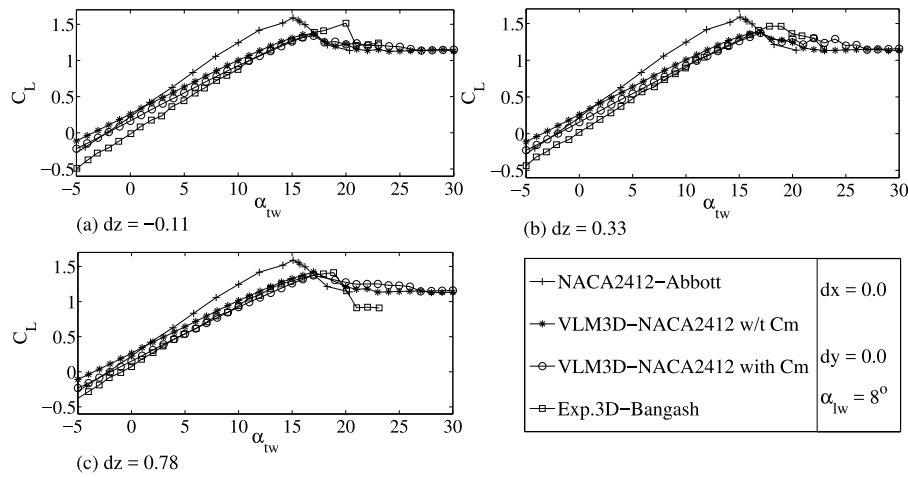


Fig. 6. Wing $C_L - \alpha_{tw}$ for different input data and for $\alpha_{lw} = 8^\circ$.

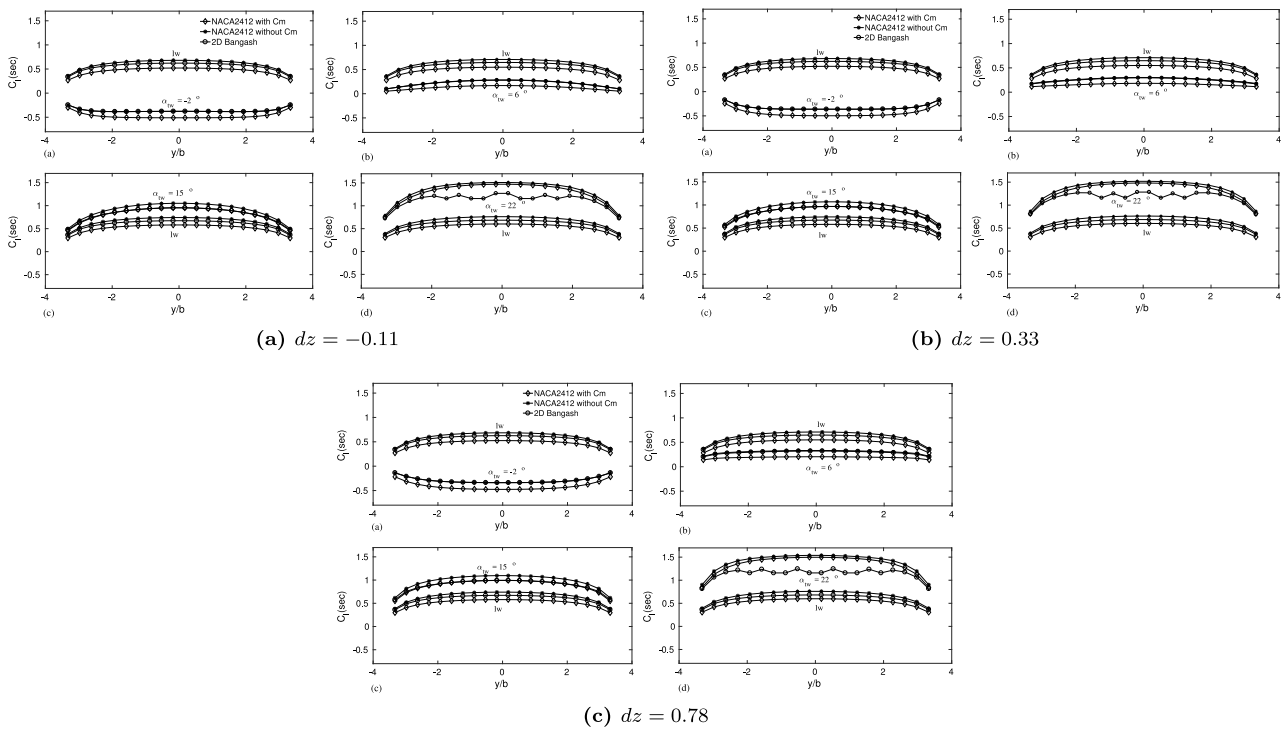


Fig. 7. Section C_l distribution for different input data for $\alpha_{lw} = 8^\circ$ and $\alpha_{tw} = -2^\circ, 6^\circ, 15^\circ, 22^\circ$.

and $dz_{lw-tw4} = \pm 0.44$. The angle of attack of the leading wing, $\alpha_{lw} = 8^\circ$ and the trailing wings undergo a sequence of angles of attack, $-5^\circ < \alpha_{tw} < 29^\circ$.

It is observed from Fig. 11 that the location of the trailing wing below or above the wing does not change its aerodynamic characteristics for the same magnitude of the vertical offset. A primary difference of the 5-wing configuration from the 2-wing configuration is the change in slope of the $C_L - \alpha$ and $C_{Di} - \alpha$ curves for the trailing wings. The first trailing wing has the largest slope and this decreases for further trailing wings. In addition to this, the zero-lift angle of attack, α_{0l} shifts from $\approx -5^\circ$, when the wing is operating individually to $\approx +5^\circ$ when 5 similar wings are operating in a configuration. Hence, the operating range of the configuration for positive lift is decreased.

However, further increasing the positive vertical offsets of the trailing wings does not affect the slope of the $C_L - \alpha$ and $C_{Di} - \alpha$ curves or C_{Lmax} or α_{0l} as shown in Fig. 12 for $\alpha_{lw} = 6^\circ$. In other

words, the advantages of the configuration shown in Fig. 11 can be obtained for a smaller angle of attack of the leading wing for the same vertical offsets of the trailing wings.

Now, for the leading wing operating at near and post-stall angles of attack, the slope of the $C_L - \alpha$ and $C_{Di} - \alpha$ curves changes but the significant change is in the further shift of the α_{0l} to $\approx 10^\circ$ as shown in Fig. 13. This means that the range of operation in the positive lift zone is further reduced.

The effect of vertical offset dz , which essentially denotes the location of the trailing wings with respect to the leading wing and various angles of attack of the leading wing, including high angles of attack is summarized in Fig. 14.

As shown by the skyblue and green curves in Fig. 14, if the magnitude of the vertical offset, dz is same, its sign, positive or negative denoting the location of the trailing wing above or below the leading wing respectively is insignificant to the change in slope of the $C_L - \alpha$ curve. For the skyblue, green, blue and red

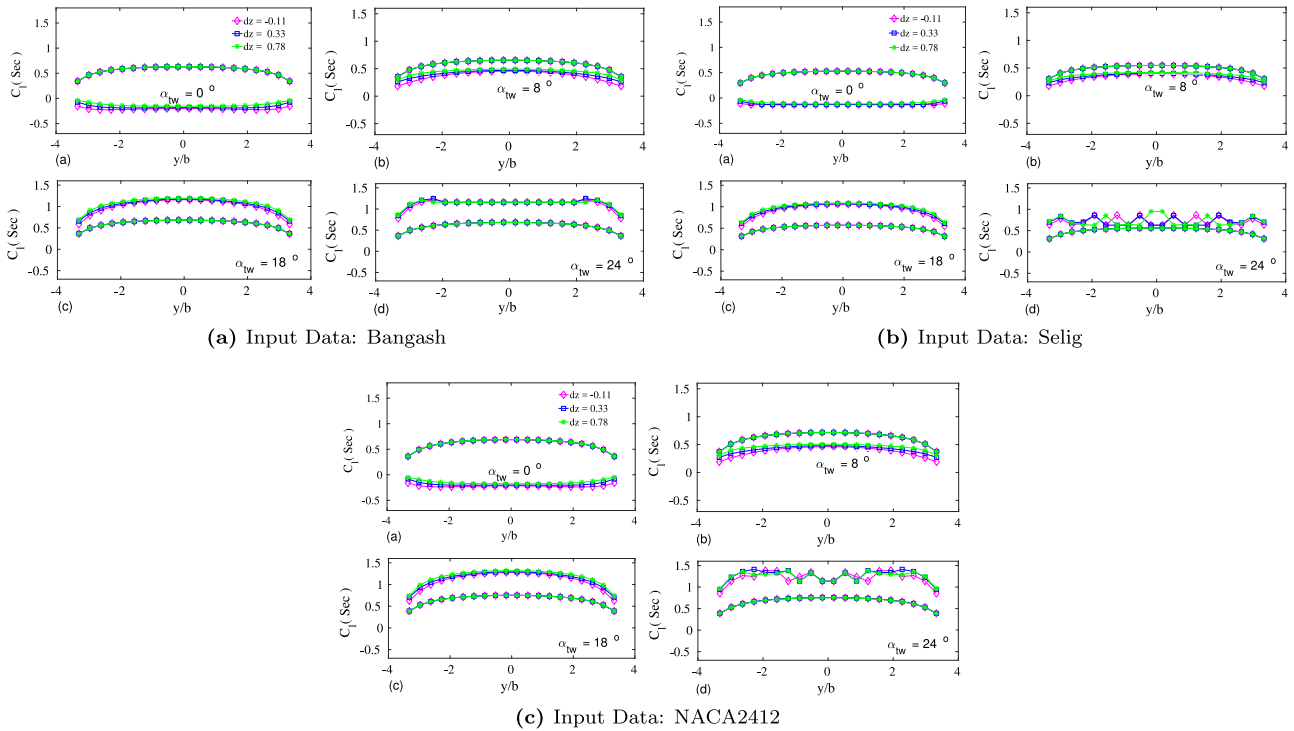


Fig. 8. Section C_l distribution for different 2D input data for $\alpha_{tw} = 8^\circ$.

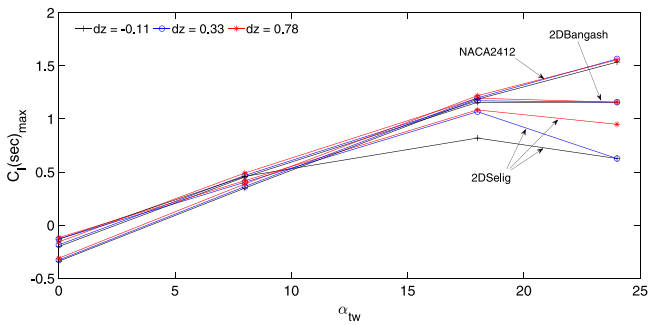


Fig. 9. Effect of input data, vertical offsets and angle of attack of the trailing wing on maximum section C_l at root section; $\alpha_{tw} = 8^\circ$.

curves, $\alpha_{tw} = 8^\circ$ but the slope changes drastically for the skyblue and green curves while the change is much more gradual for the blue and red curves since the vertical offsets between the trailing wings and the leading wing for the red curve are highest. The magenta and black curves are due to a combined effect of dz and high operating angle of attack of the leading wing.

As shown in Fig. 15, change in vertical offsets of the first trailing wing has the least effect on its aerodynamic performance compared to the wings trailing behind it. This can be attributed to the change in downwash encountered by a trailing wing, which in turn decreases the local effective angle of attack as its vertical offset with the leading wing changes. The first trailing wing receives greater airflow and rest of the trailing wings receive lesser airflow leading to changes in the strength of the flow. Delayed flow separation particularly in the last few rows of trailing wings happens due to both the above mentioned reasons. This is similar to the downwash effect on wing–tail combination of fixed wing aircraft, where the downwash effect decreases the local effective angle of attack in the tailplane to give negative lift. The combined effect of the decreased downwash and strength of the flow reduces the C_L and C_{D_i} as the offset between the individual

trailing wings and the leading wing changes. Also, the last trailing wing experiences the least induced drag.

The section C_l distribution for increasing vertical offsets between the trailing wings and the leading wing at four selected angles of attack of the trailing wings are shown in Fig. 16.

As expected the first trailing wing has the highest section C_l and it is the only wing that stalls at $\alpha = 25^\circ$ but at a higher vertical offset, e.g. $dz_{lw-tw1} = 0.78$ shown in Fig. 16c the region of stall at the root is smallest. This is also expected since with increase in vertical offset the effect of the downwash from the leading wing decreases and the stall is dominated by the effect of the high operating angle of attack of the trailing wing.

The effect of vertical offsets on the section C_l distribution for the individual trailing wings is shown in Fig. 17. Only the first trailing wing stalls at $\alpha = 23^\circ$ and $\alpha = 25^\circ$ for the highest vertical offset, $dz = 0.78$. It is therefore expected that the stall is dominated by its angle of attack rather than its vertical offset since the effect of the downwash is minimum.

The section C_l distribution on the trailing wings when the leading wing is near or at post-stall is shown in Fig. 18. It is observed from Fig. 18a for $\alpha_{tw} = 15^\circ$ that none of the 5 wings stall. The leading wing continues to operate at the maximum section C_l possible even when the trailing wings operate at $\alpha_{tw} = 0^\circ$. At $\alpha_{tw} = 25^\circ$ however, the first trailing wing is near stall much ahead of the leading wing. This can be attributed to the fact that when the angle of attack of the first trailing wing becomes greater than the angle of attack of the leading wing, say $\alpha_{tw} = 23^\circ$, due to the downwash from the leading wing there is a decrease in the distribution of the effective angle of attack of the first trailing wing but it is just about $\approx \alpha_{stall}$ allowing it to operate at the maximum section C_l but not stall.

As its angle of attack continues to increase, it operates at the highest possible C_l but does not stall even say at $\alpha_{tw} = 25^\circ$. In other words, for $\alpha > 15^\circ$, all the five wings would have stalled if operating individually. When operating in a configuration however, none of them stall and the first trailing wing operates at the highest possible section C_l . The other trailing wings including the leading wing operate at a lesser section C_l .

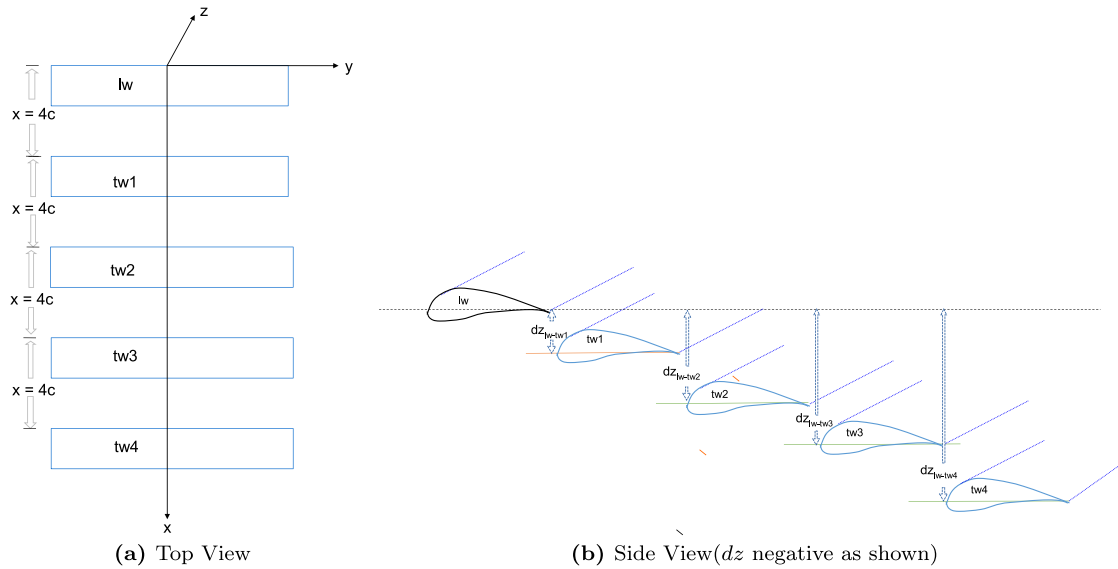


Fig. 10. Illustration of extended lead-trail formation with 5 wings.

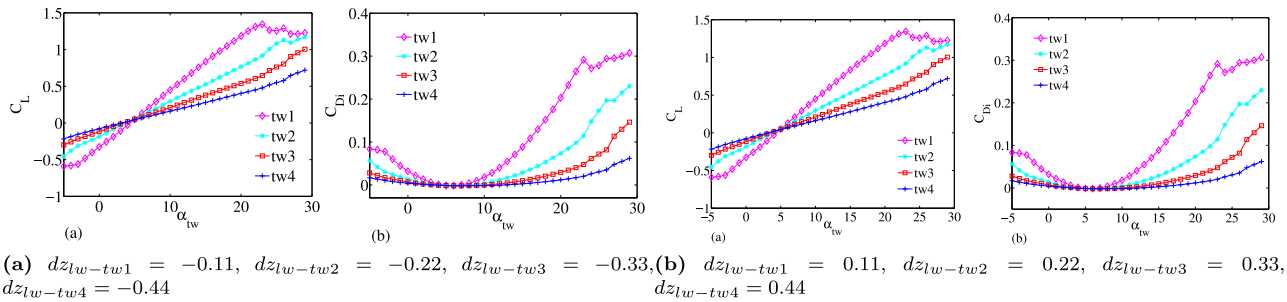


Fig. 11. 5-wing configuration; $\alpha_{lw} = 8^\circ$, $dx = 0$, $dy = 0$.

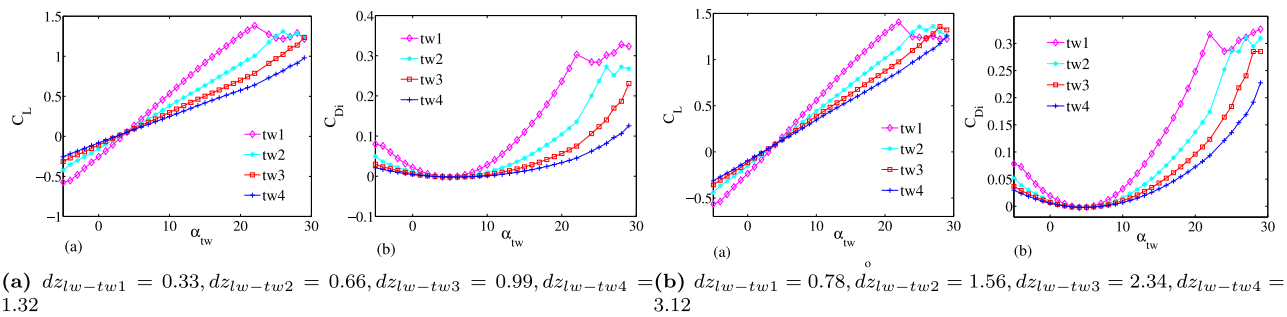


Fig. 12. 5-wing configuration; $dx = 0$, $dy = 0$, $\alpha_{lw} = 6^\circ$.

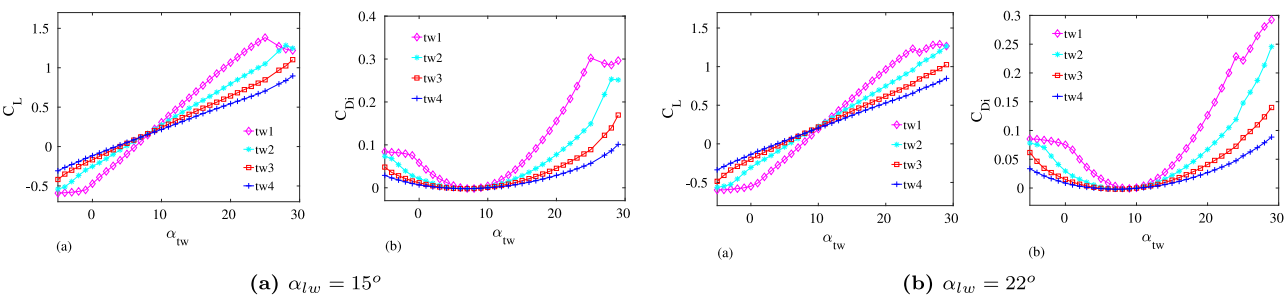


Fig. 13. Leading wing near or at post stall: $dz_{lw-tw1} = 0.33$, $dz_{lw-tw2} = 0.66$, $dz_{lw-tw3} = 0.99$ and $dz_{lw-tw4} = 1.32$.

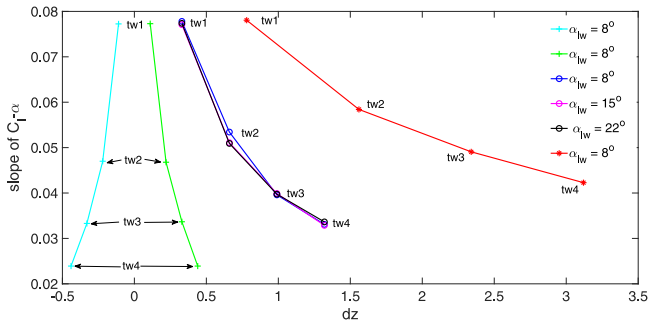


Fig. 14. Effect of vertical offsets between leading and trailing wings and angle of attack of leading wing on a 5-wing configuration. (For interpretation of the references to color in this figure legend, the reader is referred to the web version of this article.)

At $\alpha_{lw} = 22^\circ$, the root section of the leading wing stalls even at $\alpha_{tw} = 0^\circ$ resulting in a decrease in the downwash as well as two additional trailing vortices causing upwash on the trailing wings. The effect of this is maximum on the first trailing wing shown by the sharp change in the section C_l at the root section. At $\alpha_{lw} = 25^\circ$, the first trailing wing stalls and the second trailing wing begins to see a sharp increase in its section C_l at the root section.

It is therefore safe to predict that operating at post-stall angles of attack is definitely advantageous from the point of view of saving fuel as well as more wings flying in configuration provided the leading wing remains unstalled.

A comparison of the maximum section C_l with change in vertical offsets for the 2 and 5-wings configurations is shown in Fig. 19. It is seen that for the trailing wings in both configurations, the maximum section C_l increases with increase in vertical offset, dz . For a given vertical offset however, the trailing wing of the 2-wing configuration and the first trailing wing of the 5-wing configuration have similar maximum section C_l , in fact the latter's maximum section C_l is slightly more than the former's. The maximum section C_l for the remaining trailing wings of the 5-wing configuration is much lesser. It is therefore safe to suggest that

it is advantageous to operate with more wings in a configuration with a high vertical offset.

For a 5-wing configuration, the effect of a set of given vertical offsets on the maximum section C_l for increasing angles of attack of the trailing wings is shown in Fig. 20. It is observed that only the first trailing wing stalls at $\alpha \approx 24^\circ$. Hence, it is advantageous to operate with multiple wings at a high angle of attack such that none of them stall.

4. Conclusion

Analysis of a basic 2-wing and extended 5-wing lead-trail formation is carried out using an in-house numerical code, which models flow separation using local camber correction of the wing surface. The aerodynamic performance of the formations is tested for change in vertical offset wherein the trailing wing may be positioned above or below the leading wing and angles of attack of individual wings, which include both negative and post-stall angles of attack.

A trailing wing in a 5-wing configuration can operate at a higher C_l at a given α but has a lesser range. The further a wing trails the leading wing, it experiences lesser aerodynamic load. If the vertical offsets remain same, the leading wing can operate at a smaller angle of attack without compromising the aerodynamic advantages of the trailing wings. At high angles of attack, stall is delayed and it is advantageous in terms of operating at high C_l without significant C_{Di} penalty, which in turn means fuel savings. However, at such high angles of attack the range of operation is decreased.

It is advantageous to have more wings in a configuration. The last wing in a 5-wing configuration experiences almost 39% less aerodynamic load than the last wing in a 2-wing configuration. For a given angle of attack, in a 5-wing configuration, the second to fifth trailing wings experience less aerodynamic load when operating in a configuration. The last wing experiences the least induced drag and in some cases it is even found that it experiences almost zero induced drag. In a particular case, the last wing in a 5-wing configuration experiences almost 33% less induced drag than the first trailing wing.

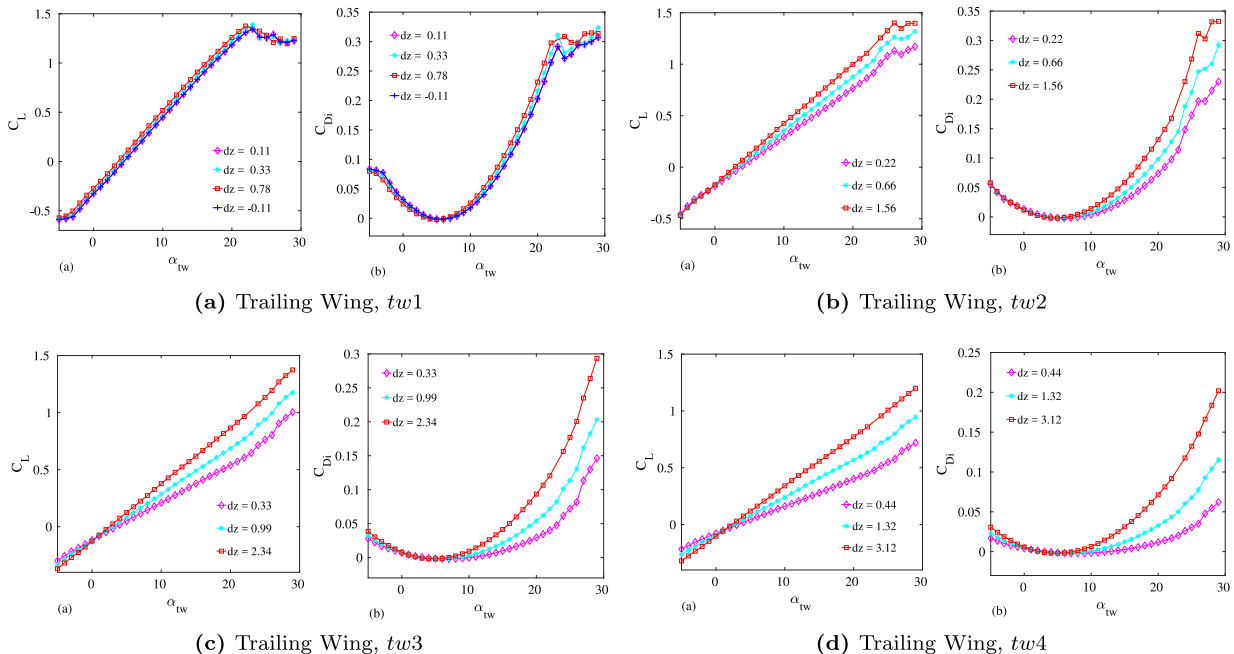


Fig. 15. 5-wing configuration; $dx = 0$, $dy = 0$, $\alpha_{lw} = 8^\circ$, airfoil: NACA2412.

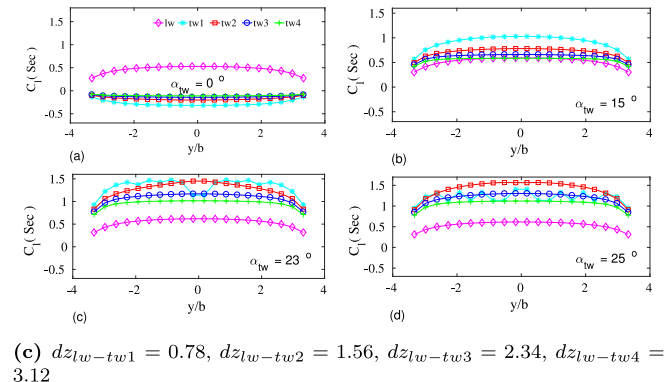
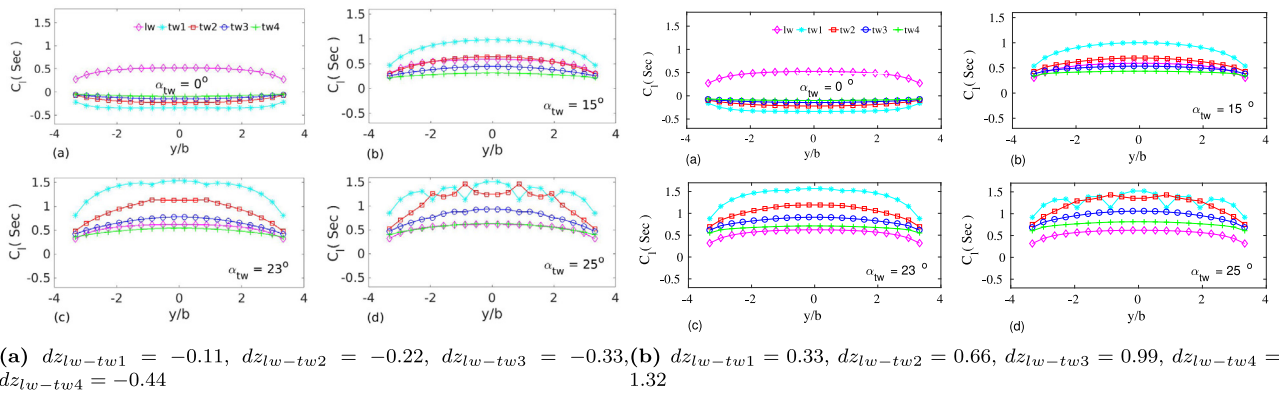


Fig. 16. Section C_l distribution on trailing wings of 5-wing configuration; $\alpha_{tw} = 8^\circ$.

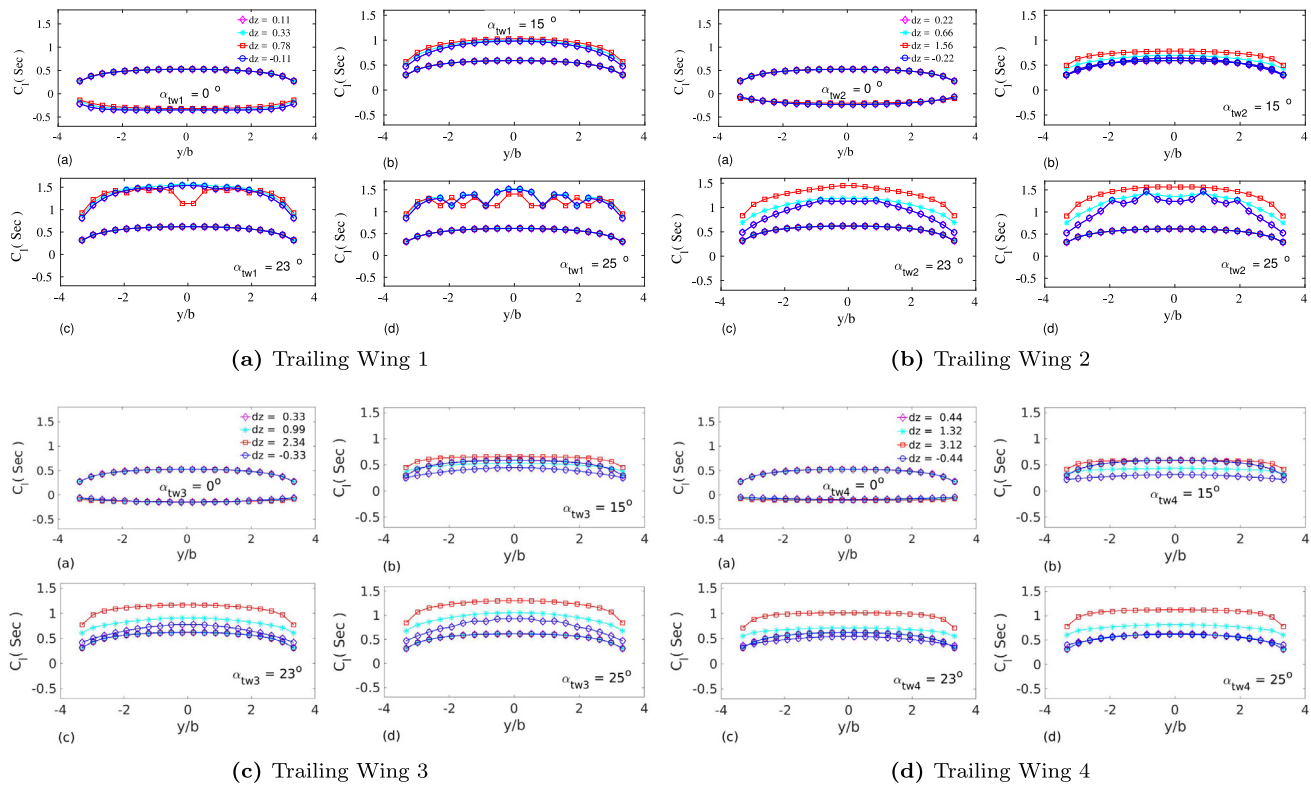


Fig. 17. Effect of vertical offsets on Section C_l distribution of trailing wings of 5-wing configuration; $\alpha_{tw} = 8^\circ$.

For an aircraft, the operating C_L is determined by mission requirements as well as safety margins, which prevent operating

at C_L close to the maximum. Therefore, the vertical offset and angle of attack of the first trailing wing should be optimally

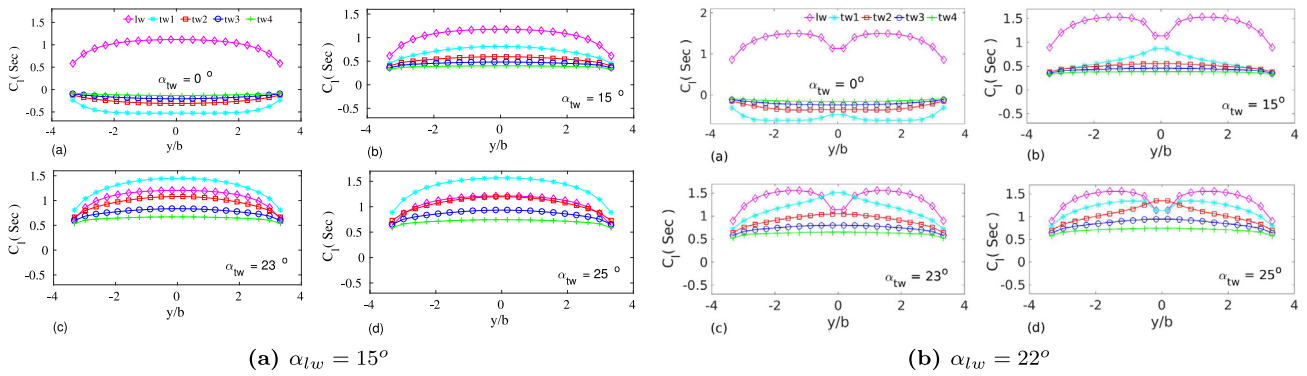


Fig. 18. Section C_l distribution on trailing wings of 5 wing formation when leading wing is near or at post stall; $dz_{lw-tw1} = 0.33$, $dz_{lw-tw2} = 0.66$, $dz_{lw-tw3} = 0.99$ and $dz_{lw-tw4} = 1.32$.

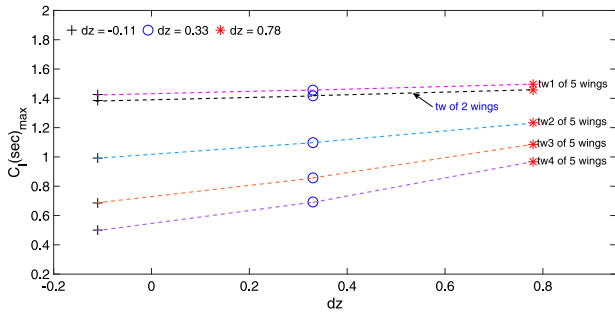


Fig. 19. Section C_l : Comparison of basic and extended lead-trail configuration.

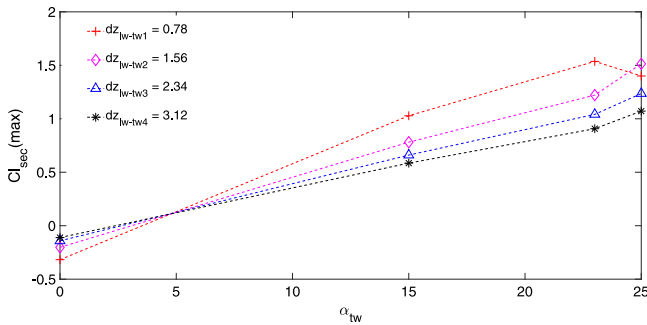


Fig. 20. Section $C_{l_{max}}$: Effect of vertical offset.

chosen such that the wing operates at the maximum possible C_l but does not stall. For example, if the first trailing wing in a 5-wing configuration has a vertical offset of 0.78 and the leading wing angle of attack is 8° then it experiences maximum C_l when operating at $\alpha = 15^\circ$. Another example is when the first trailing wing in a 5-wing configuration has a vertical offset of 0.33 and the leading wing angle of attack is 15° then it experiences maximum C_l when operating at $\alpha = 23^\circ$. There is no stall in either of these cases.

The authors believe that using the analysis presented here, feasible lead-trail configuration flight can be designed to operate at reduced range of angles of attack but sufficiently high angles

of attack for maximum savings in fuel and efficient load bearing ability of the trailing wings.

Declaration of competing interest

The authors declare that they have no known competing financial interests or personal relationships that could have appeared to influence the work reported in this paper.

References

- [1] V. Martinot, P. Rozanes, Station keeping strategies for lead-trail formation flying, in: IAF Abstracts, 34th COSPAR Scientific Assembly, The second world space congress, Houston, USA, 2002.
- [2] L.E. Buzogany, Automated control of aircraft in formation flight (Master Thesis), Air Force Institute of Technology, USA, 1992, AD-A259 020.
- [3] I.L. Bajec, F.H. Heppner, Organized flight in birds, *Anim. Behav.* 78 (4) (2009) 777–789.
- [4] C.J. Cutts, J.R. Speakman, Energy savings in formation flight of Pink-footed Geese, *J. Exp. Biol.* 189 (1) (1994) 251–261.
- [5] R.M. King, A. Gopalathnam, Ideal aerodynamics of ground effect and formation flight, *J. Aircr.* 42 (5) (2005) 1188–1199.
- [6] H.P. Thien, M.A. Moelyadi, Effects of leader's position and shape on aerodynamic performances of v flight formation, in: International Conference on Intelligent Unmanned Systems, Bali, Indonesia, 2007.
- [7] H. Weimerskirch, J. Martin, Y. Clerquin, P. Alexandre, S. Jiraskova, Energy saving in flight formation, *Nature* 413 (6857) (2001) 697–698.
- [8] R. Mukherjee, A. Gopalathnam, Post-stall prediction of multiple-lifting-surface configurations using a decambering approach, *J. Aircr.* 43 (3) (2006) 660–668.
- [9] M. Gunasekaran, R. Mukherjee, A Numerical Study of the Aerodynamics of Cessna 172 aircrafts in Echelon formation, 2014, AIAA 2014-1107.
- [10] M. Gunasekaran, R. Mukherjee, Behaviour of trailing wing(s) in echelon formation due to wing twist and aspect ratio, *Aerosp. Sci. Technol.* 63 (2017) 294–303.
- [11] M. Drela, in: T.J. Mueller (Ed.), XFOIL: An Analysis and Design System for Low Reynolds Number Airfoils, *Low Reynolds Number Aerodynamics*, in: Lecture Notes in Engineering, vol. 54, Springer-Verlag, New York, 1989, pp. 1–12.
- [12] J. Katz, A. Plotkin, *Low-Speed Aerodynamics from Wing Theory to Panel Methods*, McGraw-Hill, Inc., 1991.
- [13] W.H. Press, S.A. Teukolsky, W.T. Vetterling, B.P. Flannery, *Numerical Recipes in Fortran—the Art of Scientific Computing*, Cambridge University Press, New York, 1992.
- [14] Z.A. Bangash, R.P. Sanchez, A. Ahmed, Aerodynamics of formation flight, *J. Aircr.* 43 (4) (2006) 907–912.
- [15] Abbott, H. Ira, A.E. Von Doenhoff, *Theory of Wing Sections*, Dover, Mineola, NY, 1959.
- [16] M.S. Selig, *Summary of Low Speed Airfoil Data, Vol. 1*, SolarTech, 1995.